13 Cosmological Context

As the most luminous explosions in the universe spreading in a wide range of redshift, GRBs serve as bright beacons to probe the evolution of the universe. As a result, there is a close tie between GRBs and cosmology. GRBs within the cosmological context are discussed in this chapter. Section 13.1 describes how the properties of GRB prompt emission and afterglow evolve as a function of redshift, both from the theoretical and observational points of view. Section 13.2 discusses whether the first-generation population III stars may produce GRBs. GRBs as probes of star formation history, metal enrichment history, reionization history of the universe, as well as extragalactic background light are discussed in §13.3. Finally, the potential of applying GRBs (in conjunction with other probes) to conduct *cosmography*, i.e. to measure cosmological parameters, is discussed in §13.4.

13.1 GRB Properties as a Function of Redshift

GRBs have been detected in a very wide redshift range, from $D_{\rm L} \sim 40$ Mpc for the short GRB 170817A associated with the NS–NS merger gravitational wave event GW170817 (Abbott et al., 2017e) and $z = 0.0085$ for the long GRB 980425 associated with the Type Ic SN 1998bw (Galama et al., 1998), to $z \sim 9.4$ for the long GRB 090429B (Cucchiara et al., 2011a). This is thanks to their broad luminosity function that covers ∼8 orders of magnitude (from 10^{46} erg s^{-1} to 10^{54} erg s^{-1}) for long GRBs and ∼7 orders of magnitude (from 10^{47} erg s^{-1} to 10^{54} erg s^{-1}) for short GRBs, which allows them to be detected in a wide range of redshift. Even though the redshifts of GRBs were measured only after 1997, it took a relatively short time for them to become the top contender to break the redshift record of objects in the universe against quasars and galaxies (Fig. 13.1).

13.1.1 Prompt Emission

Theoretically, there is no straightforward prediction regarding how GRBs at higher redshifts may differ from their low-redshift brethren. This is because we still have not identified the progenitor systems of GRBs, let alone investigated their evolution with redshift. Another comment is that, unlike other cosmological objects,[1] GRBs are explosions

[1] For example, quasars are accreting super-massive black holes. Even though individual quasars can be different from case to case, statistically one would expect an evolution of quasar luminosity as a function of redshift, with factors such as black hole mass, ambient medium density, star formation feedback effect, etc. playing a role.

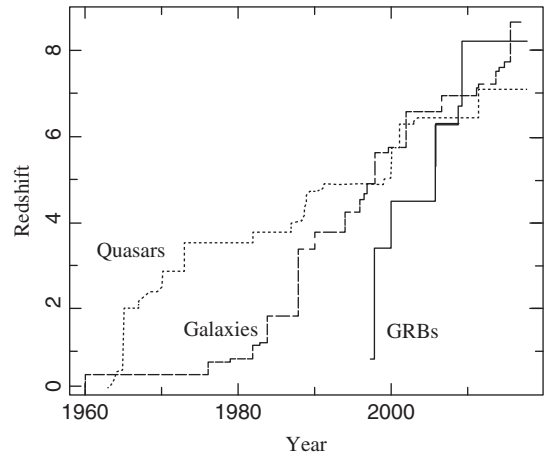

Figure 13.1 The record redshifts as a function of time for three different probes as of 2017: galaxies (dashed), quasars (dotted), and GRBs (solid). Figure courtesy Nial Tanvir.

of individual stars. There is likely no direct connection between a star that exploded at $z = 1$ and another star that exploded at $z = 5$. More importantly, the spread in the intrinsic properties is much wider than that due to the redshift evolution effect. Observationally, the redshift effect is barely noticeable.

One may ask a question: what would a GRB look like if it were moved to progressively higher redshifts? No two GRBs are identical, so it is hard to address this question directly from observations. Nonetheless, simulations can be made to "move" a GRB to progressively higher redshifts. Figure 13.2 (upper) gives an example of moving the "naked-eye" GRB 080319B at $z = 0.937$ (Racusin et al., 2008) to progressively higher redshifts (Lü et al., 2014). Starting from the prompt emission data of the GRB, one can conduct a time-dependent spectral analysis to obtain the spectral parameters (e.g. E_p, α, and β) of each time bin. Given the measured redshift z of the GRB, one can then work out the time-dependent bolometric burst luminosity through

$$L(t) = 4\pi D_{\rm L}^2(z) F(t) k, \tag{13.1}$$

with the k-correction factor

$$k = \frac{\int_{1/1+z}^{10^4/1+z} EN(E)dE}{\int_{15}^{150} EN(E)dE} \tag{13.2}$$

correcting the energy observed in the *Swift* BAT band (15–150 keV) to a broader bolometric band (1–10^4 keV).

By moving the GRB from z to a higher redshift z', one may work out the time-dependent flux of the new *pseudo GRB* through

$$F'(t') = \frac{L(t)}{4\pi D_{\rm L}^2(z') k'}, \tag{13.3}$$

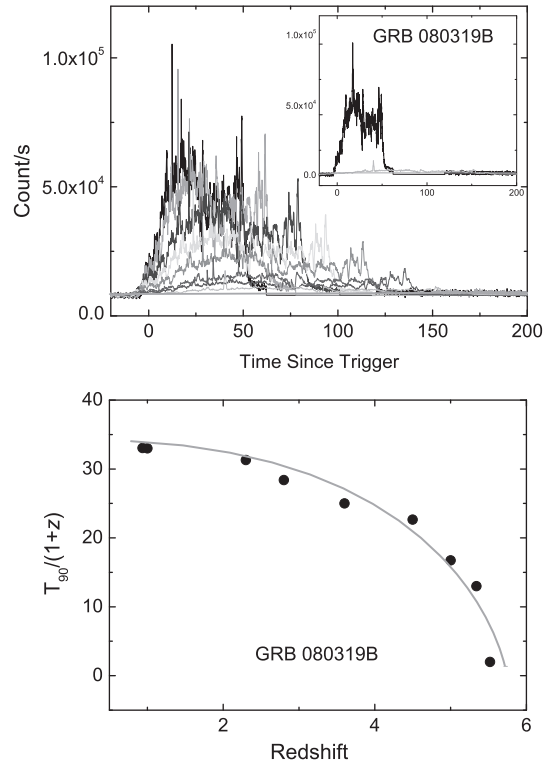

Figure 13.2 *Upper:* The simulated pseudo GRB lightcurves by moving the naked-eye GRB 080319B to progressively higher redshifts. From top to bottom, lightcurves are for $z = 0.937, 1, 2.3, 2.8, 3.6, 4.5, 5.1, 5.53$, respectively. *Lower:* The simulated $T_{90}/(1+z)$ of the pseudo GRBs as a function of z. From Lü et al. (2014).

with the factor

$$k' = \frac{\int_{1/1+z'}^{10^4/1+z'} E'N(E')dE'}{\int_{15}^{150} E'N(E')dE'} \tag{13.4}$$

correcting the bolometric luminosity to the BAT band for the pseudo GRB. By repeating the procedure, one can get the simulated lightcurves of the pseudo GRBs that mimic placing GRB 080319B at progressively higher redshifts. One can see that this bright GRB at $z = 0.937$ is observable at redshifts as high as $z \sim 6$.

One interesting feature from these simulations is that the simulated $T_{90}/(1+z)$ becomes progressively shorter as redshift increases (Fig. 13.2, lower). Above a certain redshift, it becomes *rest-frame short*, i.e. $T_{90}/(1+z) < 2$ s. This is because of a *tip-of-iceberg* effect. At high redshifts, much of the original "signal" is buried beneath the background. Only the brightest spikes are above the background noise.

Observationally, the three highest z GRBs all have $T_{90}/(1+z)$ shorter than 2 seconds: GRB 080913 at $z \simeq 6.7$ has $T_{90} \simeq 8$ s (Greiner et al., 2009), GRB 090423 at $z \simeq 8.2$ has $T_{90} \simeq 10.3$ s (Tanvir et al., 2009; Salvaterra et al., 2009), and GRB 090429B at $z \simeq 9.4$ has $T_{90} \sim 5.5$ s (Cucchiara et al., 2011a). These are all consistent with the tip-of-iceberg

effect discussed above (Lü et al. 2014; see also Kocevski and Petrosian 2013; Littlejohns et al. 2013).

The cosmological time dilation effect in prompt emission has long been speculated (e.g. Norris et al., 1994). However, the identification of such an effect took a long time. Zhang et al. (2013) identified a common narrow rest-frame band (140–350 keV) for a sample of *Swift* GRBs, and observed a clear increase of the average T_{90} (for the corresponding band) as a function of z, which is consistent with the time dilation effect.

Except for the shorter durations, other observational properties of the three highest z GRBs are not very different from their low-z brethren. Since X-rays and γ-rays from tens of keV to tens of MeV can penetrate through the universe without absorption, in principle GRBs at z up to 20–30 can be detected from Earth, if they could be generated there and could be bright enough. Due to an observational selection effect, the detected high-z GRBs must have luminosities above a certain value defined by the detector sensitivity, so that they are on average more luminous than nearby ones. The Amati/Yonetoku relations state that they are also harder. This cancels out the cosmological redshift effect, so that the high-z GRBs are not particularly soft as compared with nearby ones.

13.1.2 Afterglow

The redshift dependence of afterglow flux has been studied by several authors (Ciardi and Loeb, 2000; Gou et al., 2004). The general conclusions include the following: given the same set of burst parameters (E, Γ_0, ϵ_e, ϵ_B, p, and n or A_*), at the same observational time (say, 1 hour after the GRB trigger), the X-ray flux decreases monotonically with an increasing z (mainly due to the increase of $D_{\rm L}$). The IR and radio fluxes, on the other hand, do not degrade significantly with an increasing redshift. This is thanks to a favorable k-correction effect or a favorable time dilation effect, which cancels out the $D_{\rm L}$ effect. First, the IR and radio bands are below the peak frequency $\nu_p = \min(\nu_m, \nu_c)$ where $F_{\nu,\max}$ is achieved. For the same observational frequency band, a higher z corresponds to an intrinsically higher frequency, which is closer to ν_p. Given the positive spectral slope (1/3, 2, or 5/2) below ν_p, this effect tends to increase the observed flux. Second, given the same observational epoch $t_{\rm obs}$, the rest-frame time $t_{\rm obs}/(1+z)$ is smaller for a higher z. If the lightcurve is already in the decaying phase ($\nu > \nu_p$), this effect allows one to observe an epoch that is intrinsically brighter. Even if for $\nu < \nu_p$ when the lightcurve is still climbing, this effect does not lead to much degradation of flux since the lightcurve rising slope is usually quite shallow (Sari et al., 1998). Combining the two effects, the IR and radio fluxes do not degrade significantly with increasing redshift (Fig. 13.3).

An interesting question is regarding the circumburst medium density. Based on hierarchical models of galaxy formation, the mass and size of galactic disks are expected to evolve with redshift, so that one may have $n(z) \propto (1+z)^4$ (e.g. Gou et al., 2004). On the other hand, the radiation pressure of the massive star progenitor of the GRB may smooth any variations in the original galactic ISM number density, so that a constant density $n(z) \sim n_0 = 10^{-2}$–1 cm^{-3} may be expected (Whalen et al., 2008). The available data seem to support the second view, with no clear evolution of n with redshift.

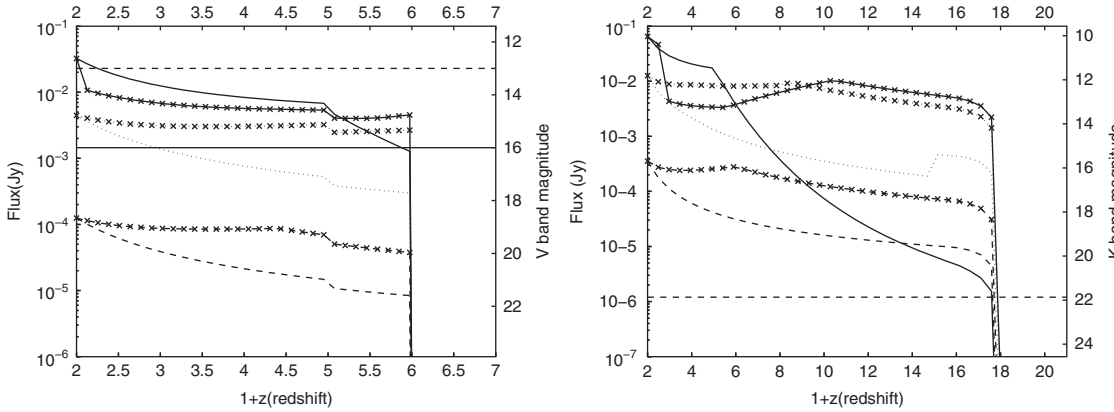

Figure 13.3 Model afterglow (including both FS and RS) flux as a function of redshift for different density profiles: $n = n_0 = 1\,\mathrm{cm}^{-3}$ (lines without symbols) and $n = n_0(1+z)^4$ (lines with symbols). *Left:* V-band ($\nu = 5.45 \times 10^{14}$ Hz); *Right:* K-band ($\nu = 1.36 \times 10^{14}$ Hz). From Gou et al. (2004).

13.2 Population III Stars and GRBs

The first stars are predicted to form at $z \sim 20$–30 (Bromm and Larson, 2004). A very exciting prospect is that the very first generation of stars in the universe might be able to generate GRBs. If this is the case, observations of very high-z GRBs would allow direct detections of these most ancient objects in the universe upon death.

Early numerical simulations (Abel et al., 2002; Bromm et al., 2002) suggested that one dark matter halo tends to form one massive Pop III star as massive as $300M_\odot$. Thanks to its zero metallicity, cooling is inefficient. This allows the star to accrete more mass to stay hydrostatic. Later simulations (e.g. Turk et al., 2009) revealed that fragmentation may occur before the core condenses to one single massive star. In these cases, the halo may contain two (or even multiple) stars, each with a smaller mass of several tens of $M_\odot$ (but is still large relative to the normal standard).

Many authors have speculated that Pop III stars may be able to make extremely long-duration and energetic GRBs (e.g. Fryer et al., 2001; Heger et al., 2003; Suwa et al., 2007; Komissarov and Barkov, 2010; Mészáros and Rees, 2010). One reservation of accepting these stars as GRB progenitors is that the extended envelope would make it difficult for a relativistic jet to emerge from the star (Matzner, 2003). Suwa and Ioka (2011) argued that, thanks to the long-lived power accretion onto the central engine, the jet may last long enough to penetrate through the stellar envelope of these stars. As of 2018, the detected high-z GRBs do not demand a Pop III star progenitor. It is possible that the GRBs formed from Pop III stars (Pop III GRBs) are fainter and are beyond reach with the currently available detectors.

One prediction for Pop III GRBs (if they exist) is that their durations should be extremely long (to allow the jet to penetrate through the large stellar envelope). The GRB luminosity may not be high (so that they may not be detected by the current detectors through rate

triggers), but the total energy of a Pop III GRB may be substantial (thanks to its long duration). It is conceivable that they may be detected with future, more sensitive detectors through imaging (fluence) triggers. If the external shock of a Pop III GRB can generate a magnetic field fraction ϵ_B comparable to that invoked in the standard GRB external shocks, then the afterglow of the first GRBs would be quite bright due to its large energy (Toma et al., 2011; Mesler et al., 2014). It remains unclear whether the seed magnetic fields in the primordial ISM/IGM are strong enough to allow the external shock to generate a strong enough magnetic field to power bright synchrotron radiation.

13.3 GRBs as Cosmic Probes

13.3.1 Star Formation History

Long GRBs originate from the deaths of a small fraction of massive stars. This raises the possibility of using GRBs to probe the star formation (SF) history of the universe.

The volumetric star formation rate $\dot{\rho}_*$ (in units of $M_\odot\ \mathrm{yr}^{-1}\ \mathrm{Mpc}^{-3}$) as a function of redshift has been probed by various SF indicators, including UV light (which directly measures the abundance of young stars), far infrared (FIR) light (which directly measures emission of the dust in the SF regions), $H\alpha$ emission (which probes the H II regions around young stars), as well as the sub-millimeter and radio continuum (which probes the ionized ISM) and line (which probes molecular clouds) emissions (e.g. Madau et al., 1998; Hopkins and Beacom, 2006; Kennicutt and Evans, 2012). Li (2008) fitted the results of Hopkins and Beacom (2006) with a piece-wise broken power law and obtained

$$\dot{\rho}_*(z) = a + b\log(1+z), \tag{13.5}$$

where

$$(a,b) = \begin{cases} (-1.70, 3.30), & z < 0.993, \\ (-0.727, 0.0549), & 0.993 < z < 3.80, \\ (2.35, -4.46), & z > 3.80. \end{cases} \tag{13.6}$$

Including also the data of high-z GRBs, Yüksel et al. (2008) obtained an approximate analytical model to delineate the SF history of the universe (upper panel of Fig. 13.4):

$$\dot{\rho}_*(z) = \dot{\rho}_0 \left[(1+z)^{a\eta} + \left(\frac{1+z}{B}\right)^{b\eta} + \left(\frac{1+z}{C}\right)^{c\eta} \right]^{1/\eta}, \tag{13.7}$$

where $\dot{\rho}_0 = 0.02 M_\odot\ \mathrm{yr}^{-1}\ \mathrm{Mpc}^{-3}$, and the smoothing factor $\eta \sim -10$. The three-segment power-law indices are

$$\begin{aligned} a &= 3.4, \\ b &= -0.3, \\ c &= -3.5, \end{aligned}$$

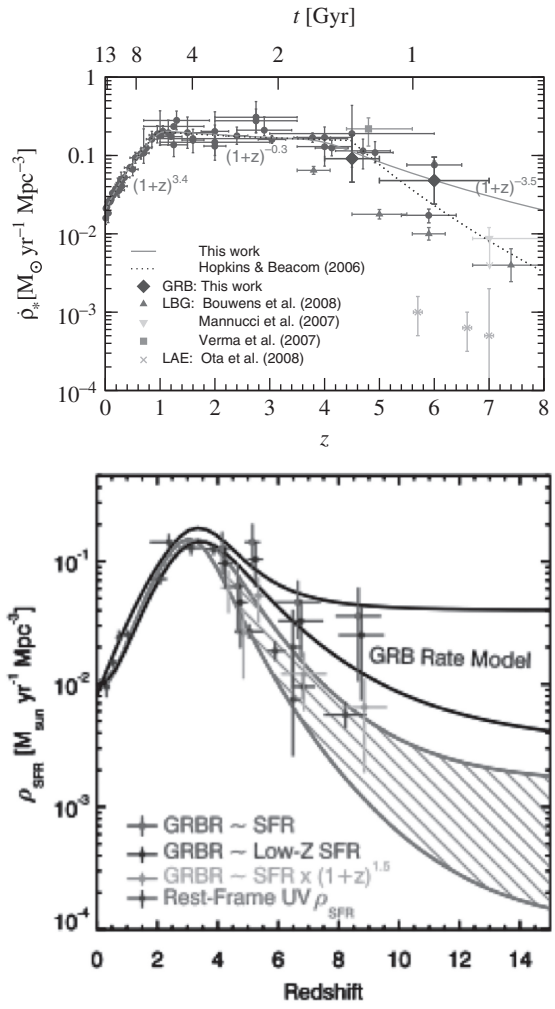

Figure 13.4 *Upper:* Star formation history measured with multiple observational probes and an analytical fit. Reproduced from Figure 1 in Yüksel et al. (2008) with permission. ©AAS. *Lower:* The SF rate probed with the rest-frame UV flux (lower solid crosses and the shaded region) and with GRBs (three different models). One can see that in any case GRBs probe a higher SF rate at high-z relative to the rest-frame UV flux, suggesting a high-z excess. Reproduced from Figure 5a in Robertson and Ellis (2012) with permission. ©AAS. A black and white version of this figure will appear in some formats. For the color version, please refer to the plate section.

with breaks at $z_1 = 1$ and $z_2 = 4$, and the coefficients

$$B = (1 + z_1)^{1-a/b} \simeq 5000,$$
$$C = (1 + z_1)^{(b-a)/c}(1 + z_2)^{1-b/c} \simeq 9.$$

All the SF indicators are subject to selection effects, and have difficulties probing the SF history at redshifts $z > 5$. The SF history in the early universe is of great interest for understanding how the universe evolves to our current form, but is poorly constrained. GRBs

offer an attractive tool for probing the star formation history of the universe, especially at high redshifts.

One question is whether GRBs are unbiased tracers of the SF history of the universe. Studies at $z < 5$ suggest that GRBs are reasonably good tracers. However, the number of high-z GRBs is in excess of the prediction based on a simple extrapolation of the current SF history to redshifts above 5 (e.g. Li, 2008; Kistler et al., 2008; Yüksel et al., 2008; Qin et al., 2010; Virgili et al., 2011b; Robertson and Ellis, 2012, see the right panel of Fig. 13.4).

There are several possibilities to account for such an apparent "high-z excess" of GRBs:

- Bromm and Loeb (2006) suggested that by including the contribution from the GRBs associated with Pop III stars, the GRB rate would increase at high z. However, the currently observed high-z GRBs that show the high-z excess are consistent with being in the same population as their nearby cousins, without showing a signature of a Pop III progenitor. The increase of the SF rate at high z is likely of a different origin.
- It is possible that the SF rate at high z is currently underestimated using the conventional probes with UV, IR, optical, sub-mm, and radio observations. The discoveries of some faint, high-z galaxies seem to support a higher SF rate at high redshifts than previously believed (e.g. Yan et al., 2012).
- One attractive proposal is the low-metallicity preference of GRBs, as supported by the data (§2.4.1) and theoretical models (§10.2.3). Assuming that the metallicity bias is the only reason for the high-z excess of the GRB rate, one may develop a simple GRB event rate density model (e.g. Li, 2008):

$$\dot{\rho}_{\rm GRB}(z) = A\Psi(z,\epsilon)\dot{\rho}_*(z), \tag{13.8}$$

where $\epsilon = Z/Z_\odot$, A is a normalization parameter, and the function (Langer and Norman, 2006)

$$\Psi(z,\epsilon) = 1 - \frac{\hat{\Gamma}(\hat{\alpha}+2, \epsilon^{\hat{\beta}} 10^{0.15\hat{\beta}z})}{\Gamma(\hat{\alpha}+1)} \tag{13.9}$$

is the fractional mass density with metallicity below $Z = \epsilon Z_\odot$, where $\hat{\Gamma}$ and Γ are the incomplete and complete gamma functions. The $\hat{\alpha}$ index is introduced from the mass density function in galaxies with a mass less than M:

$$\Phi(M) = \Phi_* \left(\frac{M}{M_*}\right)^{\hat{\alpha}} e^{-M/M_*}, \tag{13.10}$$

and the index $\hat{\beta}$ is introduced through

$$\frac{M}{M_*} = K \left(\frac{Z}{Z_\odot}\right)^{\hat{\beta}}. \tag{13.11}$$

The typical values of the two indices are $\hat{\alpha} \approx -1.16$ and $\hat{\beta} \approx 2$. This simple model is able to account for the high-z excess of GRBs (Li, 2008; Qin et al., 2010).

Cosmological numerical simulations (e.g. Choi and Nagamine, 2010) can directly derive $\Phi(z,\epsilon)$. Applying these numerical models, Virgili et al. (2011b) found that the

metallicity preference alone may not be able to account for data, and an additional evolution of the GRB luminosity function may be required.

- It is possible that the GRB event rate density may have an extra evolution factor, or that the GRB luminosity function evolves with redshift, so that high-luminosity GRBs are more common at higher redshifts. A simple $(1+z)^a$ dependence of the GRB rate has been introduced to account for the high-z excess by several authors (e.g. Qin et al., 2010; Robertson and Ellis, 2012). Virgili et al. (2011b) argued that both the metallicity effect and the evolution effect may play a role in defining the high-z excess. Physically, an evolving initial mass function (IMF) may be the origin of the evolving luminosity function of GRBs (Wang and Dai, 2011).

13.3.2 Metal Enrichment History

GRBs are good probes of their immediate environment, host galaxies, and intergalactic medium along the line of sight. For example, the chemical abundances of the host ISM and the IGM can be retrieved directly from the emission line features of GRB host galaxies, and the absorption line features of the afterglows (e.g. Prochaska et al., 2004; Chen et al., 2005). The blue optical bands carry information about *extinction*, which probes the existence of dust in the GRB emission region. The soft X-ray band is subject to absorption by interstellar metals, which is characterized by the parameter $N_{\rm H}$.[2] Figure 13.5 shows a

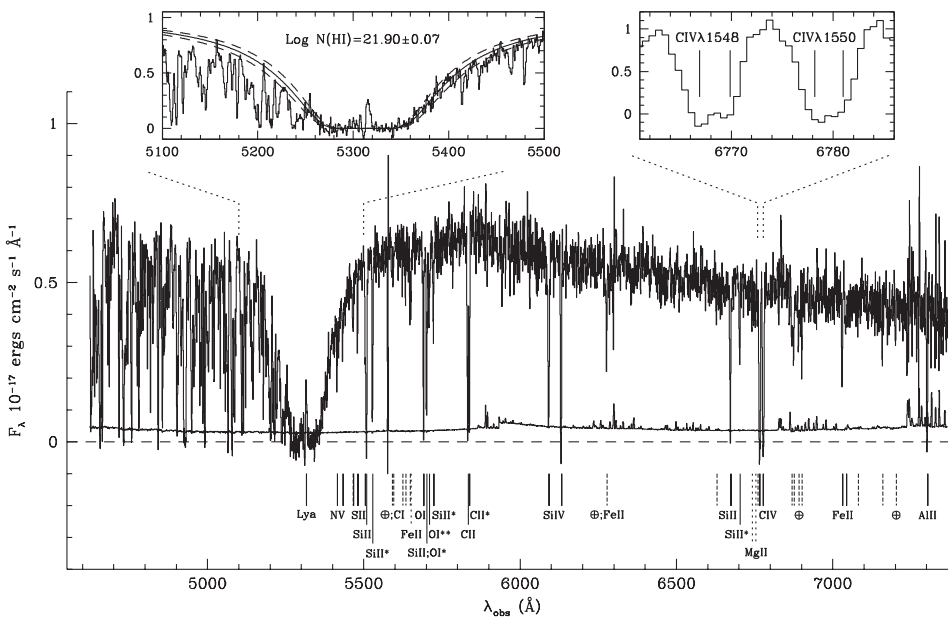

Figure 13.5 The high-resolution afterglow spectrum of GRB 030323 which shows a clear DLA and multiple metal lines. From Vreeswijk et al. (2004).

[2] The parameter $N_{\rm H}$, in units of cm^{-2}, denotes the effective neutral hydrogen column density along the line of sight of an X-ray source. However, the absorption in soft X-rays is due to metals rather than neutral hydrogen.

high-resolution afterglow spectrum of GRB 030323 (Vreeswijk et al., 2004) that clearly shows a strong Lyα absorption feature, i.e. a *damped Lyα (DLA) system*, and a wide range of low-ionization absorption lines.

In principle, by investigating the element abundances of GRBs and their evolution with redshift using these probes, one could track the metal enrichment history of the universe. In particular, if a Pop III GRB is detected, its afterglow spectrum would contain precious information about pre-galactic metal enrichment (Wang et al., 2012). The observations over the years, on the other hand, suggest a large scatter of all these probes dominated by the *intrinsic* properties of the GRBs and their circumburst environments, so that the cosmological evolution effect is not obviously retrieved (similar to other GRB properties, and as expected). Nonetheless, some interesting observational results are worth highlighting:

- The global data are consistent with the proposition that long GRBs prefer a low-metallicity environment. The long GRB hosts seem to be on average more metal poor with respect to other field galaxies with comparable redshifts.[3] Numerical simulations in order to reproduce the observed properties of GRB hosts also require a low-metallicity preference for GRBs (e.g. Niino et al., 2011). As a result, GRBs are not unbiased tracers of star formation history of the universe, especially at high redshifts.
- The GRB absorbers are characterized by an H I column density ($N_{\rm HI}$) spanning from 10^{17} cm^{-2} to 10^{23} cm^{-2} (DLAs are defined as those absorbers with $N_{\rm HI} \geq 2 \times 10^{20}$ cm^{-2}), and a metallicity spanning $10^{-2} - 1$ solar metallicity (e.g. Savaglio, 2006; Fynbo et al., 2006b; Prochaska et al., 2007).
- DLAs are related to star-forming galaxies. Observationally GRB-DLAs and QSO-DLAs have different statistical properties, but can be understood as different selection effects: GRB-DLAs probe the host galaxies of the GRBs, while QSO-DLAs are the random foreground star-forming galaxies along the line of sight of the QSOs (Nagamine et al., 2008; Fynbo et al., 2008).
- The extinction curves of GRB host galaxies are unknown, but the data of most GRBs seem to be generally consistent with the extinction curve of the Small Magellanic Cloud (SMC, e.g. Schady et al. 2010). A distinct 2175 Å bump known from the Milky Way was also discovered in the host galaxies of GRBs that have relatively high (e.g. close to solar) metallicity (Krühler et al., 2008). Making use of the power-law nature of the afterglow spectrum, efforts at directly constraining the extinction curves of GRB host galaxies have been made, resulting in extinction curves that are different from SMC, LMC, or Milky Way (Chen et al., 2006). Li et al. (2008) proposed a general analytical formula to approximate the GRB host galaxy extinction law, which was used to model the extinction data of some GRBs.
- Prochter et al. (2006) discovered a surprising increase (by a factor of 4) of incidence of Mg II absorbers along the sightlines of long GRBs as compared with quasar sightlines.

The amount of $N_{\rm H}$ is estimated based on a scaling relation between the true neutral hydrogen column density and the abundance of metals.

[3] To prove this statement is far from easy, since many selection effects may play a role. One detailed assessment of the problem is Graham and Fruchter (2013), who convincingly showed that various selection effects are not adequate for interpreting the observed apparent low metallicity of GRB hosts.

A later analysis of a larger sample by Cucchiara et al. (2013) did not confirm such an enhancement.

13.3.3 Reionization History

The Big Bang theory predicts that the early universe was hot and hydrogen was ionized until around $z \sim 1100$, when electrons and protons recombined to produce neutral hydrogen. This is the epoch of the cosmic microwave background (CMB) radiation. The universe became neutral below this redshift, but was later *reionized* by the first objects in the universe that shine in UV and X-rays (above 13.6 eV). Quasar observations suggest that reionization is nearly complete around $z \sim 6$ (Fan et al., 2006). The epoch between recombination and reionization is sometimes called the *cosmic dark ages*.

It has been speculated that the universe was reionized by sources such as the first stars and galaxies, first supernovae and GRBs, and first quasars. However, the exact detail of the reionization history is not known. Competing models predict a distinct ionization fraction as a function of redshift (Fig. 13.6, Holder et al. 2003 and references therein). In order to recover the precise history of reionization, bright beacons are needed to illuminate the dark ages.

Quasars are ideal beacons to probe reionization history below $z \sim 6$–7 (Fan et al., 2006). At higher redshifts, they become less powerful due to the rapid increase of the luminosity distance and a rapid decrease of the intrinsic luminosity of quasars (progressively smaller black holes at higher redshifts). GRBs, thanks to the favorable *k*-correction time dilation effects in the IR band (§13.1), are observable at redshifts much higher than 6, and therefore serve as a promising tool to probe the dark ages.

The reionization signature is stored in the red-damping wing of the so-called *Gunn–Peterson (GP) trough* (Gunn and Peterson, 1965). If the IGM contains a significant amount of neutral hydrogen, the afterglow spectrum blueward of the redshifted Lyα line, i.e. $\lambda \leq (1+z)1216\,\text{Å}$ (or $h\nu \geq 10.2/(1+z)$ eV), would be completely absorbed by the neutral

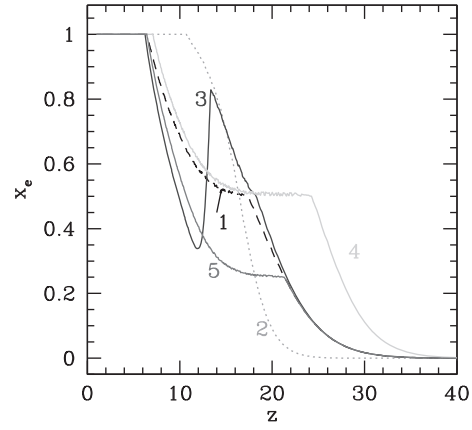

Figure 13.6 Different models of reionization history of the universe. Reproduced from Figure 1 in Holder et al. (2003) with permission. ©AAS.

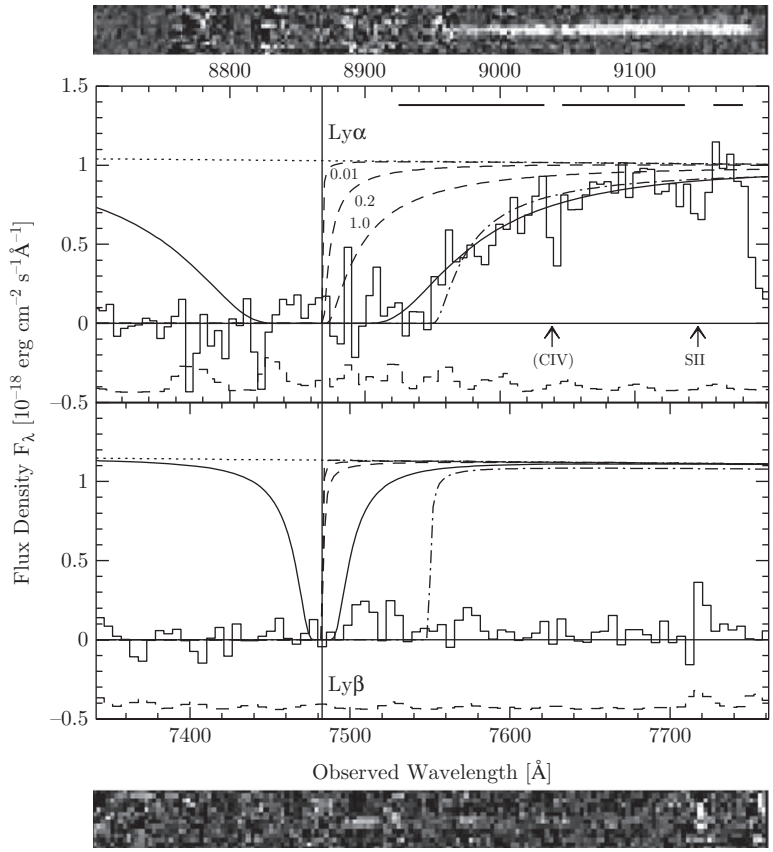

Figure 13.7 Red-damping wing of the $z \sim 6.3$ GRB 050904 fitted by the DLA (solid), GP (dashed lines with different $x_{\rm HI}$ marked in the figure), and joint DLA–GP (dash-dotted) models. From Totani et al. (2006).

hydrogen along the line of sight (from the GRB redshift z to the reionization redshift z_c). Detecting such a red-damping wing can give a measurement of the neutral fraction $x_{\rm HI}$.

Even though the GP trough has been observed in several high-z quasars (Fan et al., 2006), its identification in GRBs is challenged by the existence of a DLA in the GRB host galaxy. Figure 13.7 shows the afterglow spectrum of GRB 050904 at $z = 6.295$ taken 3.4 days after the burst (Totani et al., 2006). A clear red-damping wing is seen at the Lyα frequency at $z = 6.295$. The feature cannot be fit solely by the IGM GP effect, but is consistent with a host DLA with $\log N_{\rm HI} = 21.62$, or a combination of a DLA and the IGM GP effect.

The DLA and GP absorption effects can easily be differentiated by the frequency-dependent flux at the red-damping wing. The optical depth of a DLA can be calculated by

$$\tau_{\rm DLA}(\lambda_{\rm obs}) = N_{\rm HI}\sigma_\alpha[\nu_{\rm obs}(1+z_{\rm DLA})], \tag{13.12}$$

where $\nu_{\rm obs} = c/\lambda_{\rm obs}$ is the observed frequency, $z_{\rm DLA}$ is the redshift of the DLA, so that $\nu_{\rm obs}(1+z_{\rm DLA})$ is the cosmic-proper-frame frequency. The Lyα absorption cross section

for a rest-frame frequency ν can be written as (e.g. Peebles, 1993; Madau and Rees, 2000; Totani et al., 2006)

$$\sigma_\alpha(\nu) = \frac{3\lambda_\alpha^2 f_\alpha \Lambda_{\mathrm{cl},\alpha}}{8\pi} \frac{\Lambda_\alpha(\nu/\nu_\alpha)^4}{4\pi^2(\nu-\nu_\alpha)^2 + (1/4)\Lambda_\alpha^2(\nu/\nu_\alpha)^6}, \tag{13.13}$$

where

$$\Lambda_{\mathrm{cl},\alpha} = \frac{8\pi^2 e^2}{3 m_e c \lambda_\alpha^2} = 1.503 \times 10^9 \ \mathrm{s}^{-1} \tag{13.14}$$

is the classical damping constant,

$$\Lambda_\alpha = 3\left(\frac{g_u}{g_l}\right)^{-1} f_\alpha \Lambda_{\mathrm{cl},\alpha} \tag{13.15}$$

is the damping constant of the Lyα resonance,

$$f_\alpha = 0.4162 \tag{13.16}$$

is the absorption oscillator strength, and g_u and g_l are the statistical weights for the upper and lower levels, respectively, with

$$\frac{g_u}{g_l} = 3 \tag{13.17}$$

satisfied for Lyα. Noting that when $\nu \lesssim \nu_\alpha$, the term $(\nu-\nu_\alpha)^2 \sim 0$, one has $\sigma_\alpha(\nu) \propto \nu^{-2}$.

The red-damping wing by the IGM absorption can be modeled using the IGM optical depth (Miralda-Escudé, 1998; Totani et al., 2006)

$$\tau_{\mathrm{IGM}}(\lambda_{\mathrm{obs}}) = \frac{x_{\mathrm{HI}} R_\alpha \tau_{\mathrm{GP}}(z_{\mathrm{host}})}{\pi} \left(\frac{1+z_{\mathrm{obs}}}{1+z_{\mathrm{host}}}\right)^{3/2} \times \left[I\left(\frac{1+z_{\mathrm{IGM},u}}{1+z_{\mathrm{obs}}}\right) - I\left(\frac{1+z_{\mathrm{IGM},l}}{1+z_{\mathrm{obs}}}\right)\right], \tag{13.18}$$

where

$$1 + z_{\mathrm{obs}} \equiv \frac{\lambda_{\mathrm{obs}}}{\lambda_\alpha}, \tag{13.19}$$

$$R_\alpha \equiv \frac{\Lambda_\alpha \lambda_\alpha}{4\pi c} = 2.02 \times 10^{-8}, \tag{13.20}$$

$$\tau_{\mathrm{GP}}(z) = \frac{3 f_\alpha \Lambda_{\mathrm{cl},\alpha} \lambda_\alpha^3 \rho_c \Omega_b (1-Y)}{8\pi m_p H_0 \Omega_m^{1/2}} (1+z)^{3/2} = 3.88 \times 10^5 \left(\frac{1+z}{7}\right)^{3/2}, \tag{13.21}$$

$$I(x) = \frac{x^{9/2}}{1-x} + \frac{9}{7}x^{7/2} + \frac{9}{5}x^{5/2} + 3x^{3/2} + 9x^{1/2} - \frac{9}{2}\ln\frac{1+x^{1/2}}{1-x^{1/2}}, \tag{13.22}$$

$x_{\mathrm{HI}} \equiv n_{\mathrm{HI}}/n_{\mathrm{H}}$ is the IGM hydrogen neutral fraction, H_0 is the Hubble constant, $\rho_c \equiv 3H_0^2/(8\pi G)$ is the critical density of the universe at the present time, $\Omega_b = \rho_b/\rho_c$ is

the baryon density fraction, $\Omega_m = \rho_m/\rho_c$ is the matter density fraction, Y is helium abundance, and the IGM is assumed to be uniformly distributed between $z_{\mathrm{IGM},l}$ and $z_{\mathrm{IGM},u}$.

Figure 13.7 shows the data of the red-damping wing of GRB 050904 and the fitting results from several models, including the DLA-dominated model, IGM-only models with different x_{HI}, and hybrid models (Totani et al., 2006). Taking the redshift $z = 6.295$ determined by metal lines, a dominant DLA is required to fit the data. The IGM has an upper limit $x_{\mathrm{HI}} < 0.17\,(0.60)$ at the 68% (95%) confidence level, respectively. This is consistent with the quasar constraints that the universe is largely ionized at $z \sim 6$. Nonetheless, if one allows z as a free parameter, an IGM-dominated model with $z_{\mathrm{IGM},u} = 6.36$ and $x_{\mathrm{HI}} = 1.0$ is also allowed.

In order to apply GRBs as probes of cosmic reionization, one needs to disentangle the host DLA and the IGM absorption effects. Nagamine et al. (2008) showed that the GRB host DLA columns decrease with increasing redshift (Fig. 13.8). The mean value of DLA N_{HI} drops from 21.4 at $z = 1$ to 20.4 at $z = 10$. This is encouraging in the view that the IGM absorption becomes progressively significant at $z > 7$. If $\tau_{\mathrm{IGM}} \gg \tau_{\mathrm{DLA}}$, the data can give a better constraint on the neutral fraction of the IGM at various redshifts, leading to direct mapping of the reionization history of the universe.

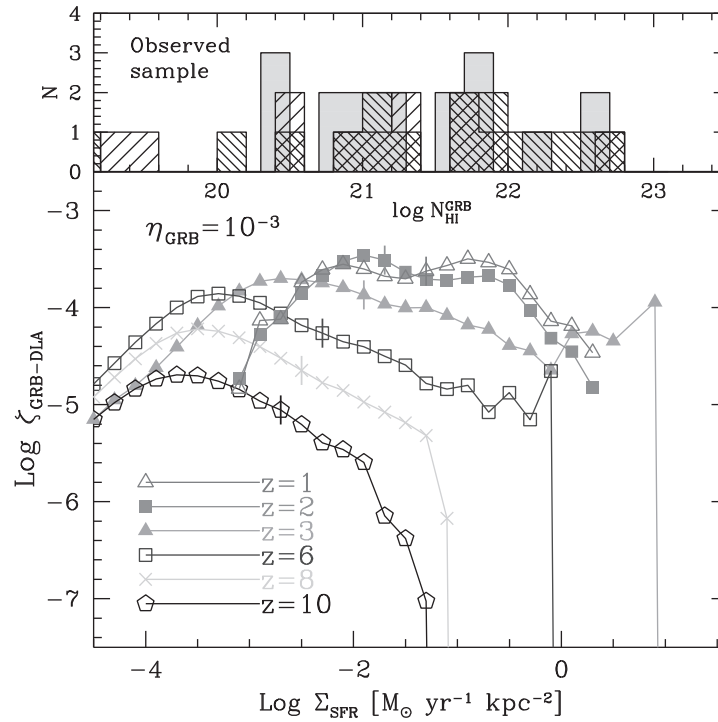

Figure 13.8 Distribution of GRB host DLAs as a function of the projected star formation rate (Σ_{SFR}) and neutral hydrogen column (N_{H}) for different redshift bins. One can see that DLAs become progressively less significant at higher redshifts. From Nagamine et al. (2008).

Observationally, a great challenge is to carry out high-resolution IR spectroscopic observations at early epochs. The observed high-z GRBs usually have their first high-resolution spectrum taken more than 10 hours after the GRB trigger, so that the afterglow has already faded significantly. Rapid follow-up observations with IR spectrographs are essential to make a breakthrough in this direction.

13.3.4 High-Energy Emission and Extragalactic Background Light

Very high energy γ-rays ($>$100 GeV) from distant astrophysical sources are subject to attenuation due to two-photon pair production through interactions with the UV/optical/IR photon background radiation in the universe, collectively known as the *extragalactic background light (EBL)*. Detecting one high-energy photon at a high enough redshift would enable posing a great constraint on the EBL (e.g. Razzaque et al., 2009).

GRBs are in principle TeV photon emitters, both from external shocks (Zhang and Mészáros, 2001b; Wang et al., 2001a), and possibly from internal emission regions as well (Razzaque et al., 2004a). Using the *Fermi* data of AGNs with redshifts up to $z \sim 3$ and GRBs with redshifts up to $z \sim 4.3$, the *Fermi* team (Abdo et al., 2010) placed stringent upper limits on the γ-ray opacity of the universe at various energies and redshifts. Some of the optimistic EBL models (e.g. the "baseline" model of Stecker et al. 2006) have been ruled out (Fig. 13.9).

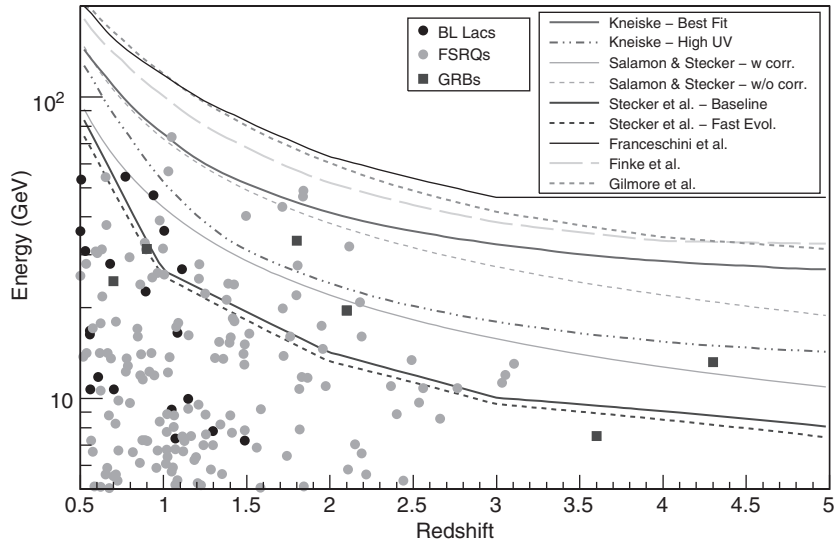

Figure 13.9 Highest energy photons from blazars and GRBs from different redshifts against the predictions of $\gamma\gamma$ optical depth $\tau_{\gamma\gamma} = 1$ for various EBL models. Some models (e.g. the "baseline" model of Stecker et al. 2006) have been ruled out by the data. (See Abdo et al. 2010 for references.) Reproduced from Figure 3 in Abdo et al. (2010) with permission. ©AAS. A black and white version of this figure will appear in some formats. For the color version, please refer to the plate section.

13.4 GRB Cosmography

13.4.1 Rationale

GRBs have been widely discussed as a tool for constraining cosmological parameters. The rationale is the following: there are several correlations invoking the energy or luminosity of GRBs (§2.6). Given a measured redshift z of the GRB, the derivations of the energy/luminosity of the GRB make use of the luminosity distance $D_{\rm L}$, which depends on the cosmological parameters. As a result, if a correlation has a physical basis and does not depend on the cosmological parameters, GRBs detected in a wide range of redshifts may serve as probes to constrain cosmological parameters. The widely used cosmic standard candles are Type Ia SNe. Systematic observations of Type Ia SNe led to the discovery of the acceleration of the universe and, hence, the existence of dark energy (Riess et al., 1998; Perlmutter et al., 1999). GRBs can potentially serve as an independent or complementary probe along with Type Ia SNe. For reviews on applying GRB relations to conduct cosmography, see Amati and Valle (2013) and Wang et al. (2015a).

To see this clearly, let us summarize various distances used in cosmology (e.g. Hogg, 1999). The *Hubble distance* can be defined as

$$D_{\rm H} = \frac{c}{H_0} \simeq 1.38 \times 10^{28}\ {\rm cm} \left(\frac{H_0}{67.3\ {\rm km\ s^{-1}\ Mpc^{-1}}}\right)^{-1} \simeq 4.46\ {\rm Gpc} \left(\frac{H_0}{67.3\ {\rm km\ s^{-1}\ Mpc^{-1}}}\right)^{-1}, \quad (13.23)$$

where H_0 is the Hubble constant (the current expansion rate of the universe), which has a measure (67.3 ± 1.2) km s^{-1} Mpc^{-1} $\simeq (2.18 \pm 0.04) \times 10^{-18}$ s^{-1} according to the Planck Mission Collaboration (Planck Collaboration et al., 2014). Generally writing

$$\Omega_m + \Omega_k + \Omega_{\rm DE} = 1, \quad (13.24)$$

as is required by the Friedmann equation, one can define a general *Hubble parameter*

$$E(z) = \frac{H(z)}{H_0} = \sqrt{\Omega_m (1+z)^3 + \Omega_k (1+z)^2 + \Omega_{\rm DE} f(z)}, \quad (13.25)$$

where Ω_m, Ω_k, and $\Omega_{\rm DE}$ are the energy density fraction of matter, curvature, and dark energy, respectively. For the standard ΛCDM model, one has

$$\Omega_{\rm DE} = \Omega_\Lambda, \quad f(z) = 1. \quad (13.26)$$

In general, the line-of-sight *comoving distance* is defined as

$$D_c(z) = D_{\rm H} \int_0^z \frac{dz'}{E(z')}. \quad (13.27)$$

The *transverse comoving distance*, which is defined as the comoving distance between two points at the same redshift divided by their angular separation, is

$$D_{\rm M}(z) = \begin{cases} \frac{D_{\rm H}}{\sqrt{\Omega_k}} \sinh\left(\sqrt{\Omega_k}\frac{D_c(z)}{D_{\rm H}}\right), & \Omega_k > 0, \\ D_c(z), & \Omega_k = 0, \\ \frac{D_{\rm H}}{\sqrt{|\Omega_k|}} \sin\left(\sqrt{|\Omega_k|}\frac{D_c(z)}{D_{\rm H}}\right), & \Omega_k < 0. \end{cases} \tag{13.28}$$

The *angular distance* is

$$D_{\rm A}(z) = \frac{D_{\rm M}(z)}{1+z}; \tag{13.29}$$

the *luminosity distance* is

$$D_{\rm L}(z) = D_{\rm M}(z)(1+z); \tag{13.30}$$

and the *light-travel distance* is

$$D_{\rm T}(z) = D_{\rm H}\int_0^z \frac{dz'}{(1+z')E(z')}. \tag{13.31}$$

Let us take the Ghirlanda relation as an example (§2.6.2). The relation $E_{p,z} \propto E_\gamma^{0.7}$, if proven physical, may be used to constrain cosmological parameters (Dai et al., 2004; Ghirlanda et al., 2004a). Based on the correlation, with a measured z, E_p, and t_j, one can derive E_γ and then $E_{\gamma,\rm iso}$ based on the correlation (not through $D_{\rm L}$). One can then derive $D_{\rm L}$ from the $E_{\gamma,\rm iso}$ inferred from the measured $E_{p,z}$ through the correlations, and hence the *distance modulus*

$$\mu = 5\log\left(\frac{D_{\rm L}}{10\ {\rm pc}}\right) \tag{13.32}$$

based on the observed γ*-ray* fluence. One can then plot a *Hubble diagram*, μ vs. $(1+z)$, of GRBs (Fig. 13.10). This observed Hubble diagram can then be compared with the predicted diagrams using Eq. (13.30) with different cosmological parameters. The best fit to the data would give constraints on the cosmological parameters. The CMB data strongly suggest a flat universe, so that $\Omega_k = 0$. The GRB Hubble diagram can then lead to a constraint on $(\Omega_m, \Omega_\Lambda)$ in the standard ΛCDM model, and the dark energy parameter w in the more general wCDM dark energy model (Dai et al., 2004; Ghirlanda et al., 2004a), with

$$f(z) = \exp\left[3\int_0^z \frac{(1+w(z''))dz''}{1+z''}\right] \tag{13.33}$$

in Eq. (13.25) for an arbitrary $w \neq -1$. The model is reduced to the standard ΛCDM model when $w = -1$.

Early efforts for constructing GRB Hubble diagrams include Schaefer (2003) (using the L–τ and L–V relations, §2.6.6 and §2.6.7) and Bloom et al. (2003) (using the Frail relation, §2.6.5). The quality of those Hubble diagrams was not good enough to conduct cosmography. After Ghirlanda et al. (2004b) claimed a tighter correlation (§2.6.2), Dai et al. (2004) and Ghirlanda et al. (2004a) independently showed that the GRB Hubble diagram derived from this relation is good enough to constrain cosmological parameters, even though not with the precision of SN Ia standard candles. Later, Liang and Zhang (2005) discovered

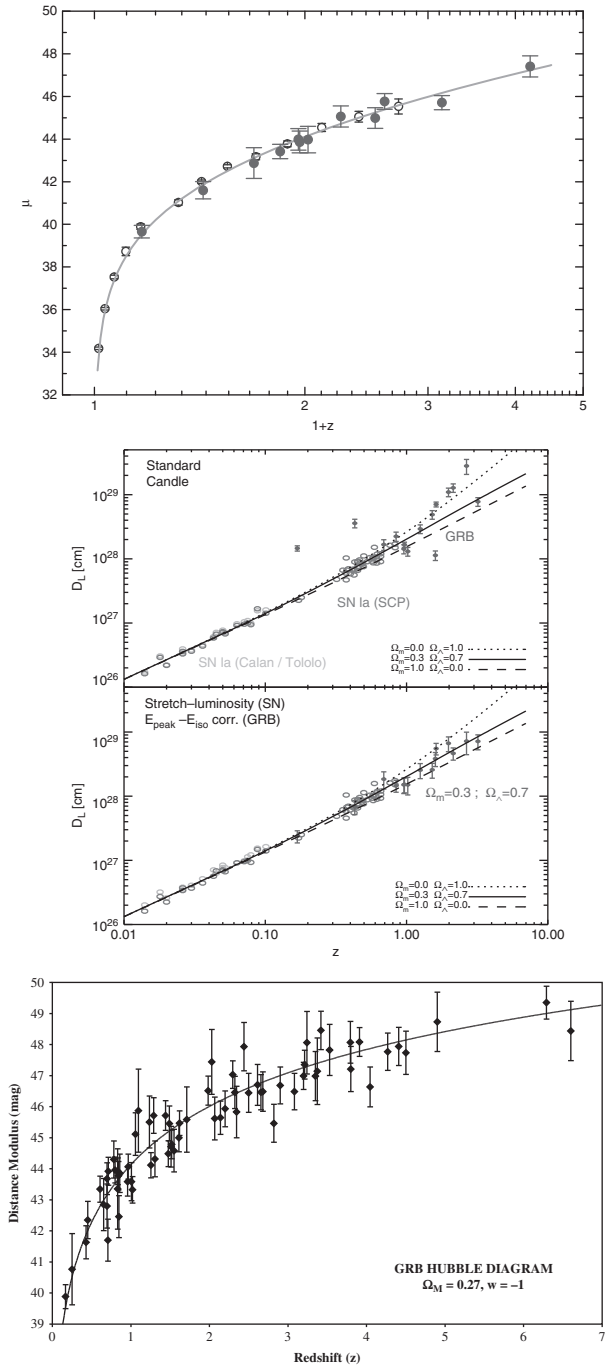

Figure 13.10 GRB Hubble diagrams constructed by various authors. The top two were based on the Ghirlanda relation, and the last one was derived using several different relations. *Upper:* Reproduced from Figure 2 in Dai et al. (2004) with permission. ©AAS. *Middle:* Reproduced from Figure 1 in Ghirlanda et al. (2004a) with permission. ©AAS. *Lower:* Reproduced from Figure 7 in Schaefer (2007) with permission. ©AAS.

a $E_{\rm iso}$–E_p–t_b three-parameter correlation (§2.6.3) and applied the correlation to perform cosmography and reached a similar precision as the Ghirlanda relation. Since then, many investigations have been carried out to conduct GRB cosmography or to combine the GRB candle and other probes to jointly constrain cosmological parameters (e.g. Schaefer, 2007; Wang et al., 2007a; Amati et al., 2008).

13.4.2 Issues and Progress

There are several issues inherent to the problem of GRB cosmography.

First, due to the *intrinsic* dispersion of the GRB correlations, the GRB candles are much less standard than the SN Ia candle. This is because the physics of GRB prompt emission is much messier than the explosion physics of Type Ia SNe. As discussed in Chapter 9, the composition, energy dissipation mechanism, and radiation mechanism are all open questions in the GRB prompt emission physics. Type Ia SNe, on the other hand, are believed to be generated from the nuclear explosion of white dwarfs, likely with mass close to the Chandrasekhar mass limit. The emission mechanism of GRBs is non-thermal. The typical emission energy E_p of the spectrum not only depends on the luminosity of the emission, but also depends on some poorly measured parameters such as bulk Lorentz factor, characteristic electron Lorentz factor, magnetic field strength, etc. The SN emission, on the other hand, is thermal with a well-defined temperature. As a result, the Type Ia SNe emission physics are cleaner and can be more easily "standardized".

It is therefore not surprising that cosmography efforts using GRB data alone so far have not led to better constraints on the cosmological parameters compared with other methods (e.g. SNe Ia and CMB) (Schaefer, 2007; Amati et al., 2008). It is possible that GRBs do not have a tight enough standard candle to perform cosmography. The scatter of the correlations is not due to a small sample size or the calibration issue, but is due to the intrinsic uncertainties inherited in GRB physics. If so, we may have already reached the limit of GRB cosmography and the parameter space constrained by the GRB candles cannot be significantly improved further.

One attractive feature of using GRBs as cosmography tools is that they can be detected at much higher redshifts than SNe Ia. Even though GRBs alone cannot make robust constraints on cosmological parameters, when combined with other probes GRBs can extend the Hubble diagram to higher redshifts and, hence, give better constraints on the evolution of cosmological parameters, revealing the nature of dark energy. Detailed analyses in this direction indeed showed that GRBs are nice complementary tools for conducting cosmography (e.g. Wang et al., 2007a).

The second issue is that GRB cosmography suffers the so-called "circularity" problem. Essentially, every GRB correlation invokes $E_{\gamma,\rm iso}$ or $L_{\gamma,\rm iso}$. Therefore, when deriving a particular correlation, a particular cosmology (usually the standard ΛCDM cosmology) has been used. One can then argue that it is not surprising that GRB cosmography also leads to the same ΛCDM model. To avoid this problem, Liang and Zhang (2005) explored a range of cosmologies in a wide parameter space, recalibrated their three-parameter correlation within each cosmology, and calculated the goodness of the relationship within each cosmology by χ^2 statistics. One can then construct a relation that is weighted by the goodness

of each cosmology-dependent relationship, and use this cosmology-weighted relationship to conduct cosmography.

A related problem is that it is not easy to calibrate GRB candles using the GRB data alone. A robust calibration (e.g. for SNe Ia) requires a low-z sample. However, the nearby GRBs tend to have much lower luminosities than their cosmological cousins, and may have a different physical origin (§10.2.5). One suggested method is to invoke a narrow redshift bin to partially calibrate the correlation (Liang and Zhang, 2006a; Ghirlanda et al., 2006). This method can only calibrate the indices of the correlations. The coefficient of the correlation, on the other hand, still depends on the adopted cosmological parameters and can only be "marginalized". Later Liang et al. (2008b) (see also Kodama et al. 2008) proposed applying SN Ia data in the same redshift range as GRBs to calibrate GRB candles. Applying the distance moduli of SN Ia and assigning them to GRBs at the same redshifts, one can derive a cosmology-independent calibration to the GRB candles. This method also naturally solves the circularity problem. The derived cosmological parameters using the calibrated candles with this method are found to be consistent with the concordance model (the standard ΛCDM model) (Liang et al., 2008b).

13.4.3 Other GRB-Related Cosmography Methods

If GRBs are associated with other signals that carry independent cosmological information, then GRBs may become a powerful tool for conducting cosmography. The following two probes are promising candidates to conduct GRB-related cosmography in the future.

First, compact-star-merger gravitational wave events are ideal "standard sirens" thanks to their unique "chirp" signal during the inspiral phase (Abbott et al., 2017a). The joint detection of GW170817 and GRB 170817A (Abbott et al., 2017b) allows an independent measurement of the luminosity distance $D_{\rm L}$ of the source based on the gravitational wave data and the recession velocity inferred from measurements of the redshift using the electromagnetic data. This led to a direct measurement of the Hubble constant $H_0 = 70.0^{+12.0}_{-8.0}$ km s^{-1} Mpc^{-1} without the need of introducing the cosmic "distance ladder" (Abbott et al., 2017a). Detecting several *standard siren* events at different distance scales with electromagnetic counterparts would provide a precise measurement of cosmological parameters (Nissanke et al., 2010).

Another interesting probe of cosmological parameters is the *dispersion measure* (DM) of a cosmological transient source. Ioka (2003) discussed the possibility of making use of the DM from GRB radio afterglows to serve as a cosmic probe. In practice, lacking a sharp pulse-like signal, a measurement of DM would be difficult. The discovery of *fast radio bursts* (FRBs, Lorimer et al. 2007; Thornton et al. 2013) and identification of their cosmological origin (Chatterjee et al., 2017; Marcote et al., 2017; Tendulkar et al., 2017) makes it potentially possible to apply the DM information to probe cosmology. In particular, there have been suggestions of possible associations between GRBs and FRBs (Zhang, 2014; Bannister et al., 2012; Metzger et al., 2017). If such associations indeed exist, the combination of the z information (obtained from the GRB observations) and DM information (obtained from the FRB observations) would help to constrain some cosmological parameters (e.g. Deng and Zhang, 2014a; Gao et al., 2014; Zhou et al., 2014).

More specifically, the IGM portion of DM is directly related to $E(z)$ through (Deng and Zhang, 2014a; Gao et al., 2014)

$$\langle \mathrm{DM_{IGM}}(z) \rangle = \frac{3cH_0\Omega_b f_{\mathrm{IGM}}}{8\pi G m_p} \int_0^z \frac{\chi(z')(1+z')dz'}{E(z')}, \tag{13.34}$$

where

$$\chi(z) \simeq \frac{3}{4}\chi_{e,\mathrm{H}}(z) + \frac{1}{8}\chi_{e,\mathrm{He}}(z) \tag{13.35}$$

is the ionization fraction of electrons ($\chi_{e,\mathrm{H}}(z)$ and $\chi_{e,\mathrm{He}}(z)$ are the ionization fractions of hydrogen and helium, respectively), Ω_b is the current baryon mass fraction of the universe, and f_{IGM} is the fraction of baryon mass in the intergalactic medium. The method can be applied as long as the redshifts of FRBs can be measured through other methods.